Biomedical Materials

ACCEPTED MANUSCRIPT

<i>In Vitro</i> and <i>In Vivo</i> biocompatibility study on acellular sheep periosteum for guided bone regeneration

To cite this article before publication: Jing He *et al* 2019 *Biomed. Mater.* in press https://doi.org/10.1088/1748-605X/ab597f

In Vitro and *In Vivo* Biocompatibility Study on Acellular Sheep Periosteum for Guided Bone Regeneration

Jing He[a,b] , Zhenning Li[c], Tianhao Yu[b], Weizuo Wang[b], Meihan Tao[b], Shilin Wang[b], Yizhan Ma[b], Jun Fan[b], Xiaohong Tian[b], Xiaohong Wang[b], Rabia Javed[b], Qiang Ao[b,d] *

[a] Center of Implant Dentistry, School of Stomatology, China Medical University, Shenyang 110002, China.

[b] Department of Tissue Engineering, China Medical University, Shenyang 110122, China.

[c] Department of Oral Maxillofacial Surgery, School of Stomatology, China Medical University, Shenyang 110002, China.

[d] Institute of Regulatory Science for Medical Device, Engineering Research Center in Biomaterial, Sichuan University, Chengdu, 610064, China

* Corresponding Author

Corresponding author:

Qiang Ao,

Department of Tissue Engineering, China Medical University, Shenyang, China

Postal address: No.77 Puhe Road, Shenyang North New Area, Shenyang, China. 110122

E-mail: aoqiang@tsinghua.edu.cn

Telephone number: +86 02431939710

Fax number: +86 02431939710

ABSTRACT

This study addresses the fabrication of an extracellular matrix material of acellular sheep periosteum, and systematic evaluation of its biocompatibility to explore its potential application in guided bone regeneration. Sheep periosteum was harvested and decellularized by a combined decellularization protocol. The effectiveness of cell removal was proved and residual α-Gal antigen was also quantitively detected. Then, mouse MC3T3-E1 cells were seeded onto the acellular periosteum. Scanning electron microscope (SEM) was used to record the whole process of cell adhesion. CCK-8 assay suggested that the acellular periosteum not only had zero toxic effect on pre-osteoblasts, but played a positive role in cell proliferation. It was also tested that whether the acellular periosteum possess favorable osteogenesis induction activity attributed to ALP assay and quantitative real-time PCR (Col I, Runx2, OCN) assay. *In vivo* study of subcutaneous implantation test using SD rats was performed to detect the changes of IL-2, IFN-γ, IL-4 in serum and elucidate the host's local response to acellular periosteum through HE and immunohistochemical staining. The results show that acellular sheep periosteum did not elicit a severe immunogenic response via Th1 pathway unlike fresh sheep periosteum. In conclusion, acellular sheep periosteum possesses favorable biocompatibility to be employed for guided bone regeneration.

Keywords: acellular periosteum; xenograft; guided bone regeneration; extracellular matrix; biocompatibility; immunoinflammatory reaction

1. Introduction

Alveolar bone and jaw bone defects, ascribed to inflammation, trauma, tumors, congenital factor and disuse-atrophy, are one of the most common clinical symptoms that exist in dental implantology, oral maxillofacial surgery and orthopedics. For patients of alveolar bone or jaw bone defects, the technique of guided bone regeneration (GBR) is often conducted for bone mass recovery. GBR is an extensively described alveolar ridge augmentation technique which has shown excellent reproducibility and high long-term success rates based on high-evidence-level publications [1]. The technical principle is that different cellular components in the tissue have varying rates of migration into a wound area during healing period in which the rates of fibroblasts are much faster than those of bone cells [2]. As a result, GBR barrier membranes are applied to prohibit soft tissue invasion and offer bone tissues in the bone defect area with adequate growing space [3]. Hence, the properties and biological responses of the membrane assuredly play a vital role in the technique of GBR.

As an accessorial anatomy of the bone, periosteum has a very close relationship with bone formation and reconstruction. It is not only a source for progenitor cells and local growth factors, but also a natural scaffold to recruit cells and biological factors [4]. Periosteal autografts have also exhibited promising results when used to promote bone repair [5]. Also, due to autologous source limitation, more and more researches focus on developing biomimetic methods to synthesize artificial periosteum which better imitates native periosteum in structure and function [6-11].

However, there is no tissue engineering approach that can fabricate the unique natural three-dimensional structure that contains the periosteum-specific extracellular matrix (ECM) components which are essential for bone regeneration and reconstruction [12]. Recently, the application of tissue-derived ECM materials has become increasingly popular in tissue engineering and regenerative medicine[13]. The decellularization processes have been conformed to efficiently remove cell components which are supposed to have immunogenicity to the host, while retaining the naturally occurring three-dimensional structure and tissue-specific bioactive components[14].

The source of allogeneic decellularized tissues is still far more limited compared to xenogeneic ones. Given that both allogeneic and xenogeneic transplantation would lead to the occurrence of immune rejection due to reaction between those specific antigens in grafts and the antibodies in the host, and as most antigens within the grafts exist on the cell surface, the process of cell removal is required as thorough as possible in both allogeneic and xenogeneic materials. Then, xenogeneic tissues, compared to allogeneic tissues, are supposed to have more advantages such as highly wider tissue sources, less acquisition costs and broader application prospects. Although some studies argued that tissue antigenicity represents the principal barrier towards use of unfixed xenogeneic ECM biomaterials in clinical practice due to its ability to stimulate recipient graft-specific adaptive immune responses [15-17], Dalgliesh et al. [18] established that recipient graft-specific adaptive humoral immune response could be overcome as long as the vast majority of lipid antigens, at least 92% of all, are sure to be removed while implanting xenogeneic extracellular matrix scaffolds. In addition, large number of studies suggest that no significant differences between xenogeneic and allogeneic materials were noted according to the treatment effects and the immunological inflammatory response detection [19-22].

In our previous study, sheep periosteum was decellularized and physico-chemically characterized for the application in GBR. We also performed animal experiments of GBR using a rabbit cranial defect model. The results of micro-CT and histological detections indicated that the acellular periosteum not only effectively prevented the ingrowth of fibrous connective tissues, but also potentially facilitated bone regeneration inside the bone defect sites [23]. To further confirm the effect of acellular periosteum at the cellular level, in the present study, we aim to detect the biocompatibility of an acellular sheep periosteum for further applications in GBR. Firstly, acellular sheep periostea were successfully fabricated with a combined traditional decellularization protocol, and the decellularization effectiveness was evaluated. Secondly, mouse MC3T3-E1 cells, which are osteoblast precursor cells, were cultivated with the acellular periosteum to study its influence on osteoblast proliferation and osteogenesis differentiation *in vitro*. Finally, the acellular periostea were subcutaneously implanted into the backs of rats to explore whether it would elicit immuno-inflammatory responses *in vivo*.

2. Materials and methods

2.1 Acellular sheep periosteum harvest

The holistic technical route of the present study is delineated in Fig.1. Fresh sheep tibiae were harvested within less than 2 h after sacrifice from one of the local halal slaughter houses. Fresh periosteum (FP) was stripped from the bone surface carefully and intactly using a periosteal detacher. Decellularization process was performed to fabricate acellular periosteum (AP) as follows: First, freeze-thaw cycle was repeated for 3 times in a way that every time FP was frozen at -80 ℃ for no less than 6 h and then thawed in a 37 ℃ water bathe for about 30 min. Next, the

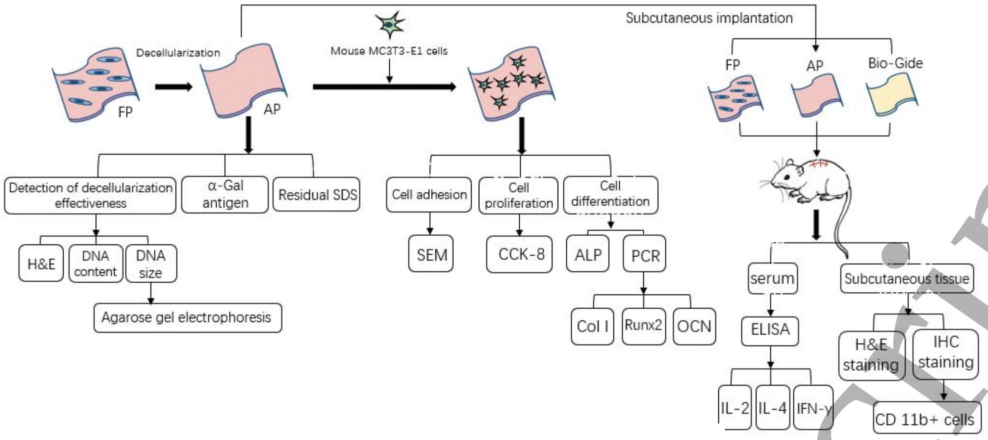

Fig. 1. Schematic flow chart of this study.

samples were treated with 1% (vol/vol) Triton X-100 (Sigma, USA) for 12 h and 0.2% (wt/vol) SDS (Sigma, USA) for 6 h under agitation (100 rpm) in a plate shaker. Then, samples were treated with DNase (100 U/ml, Sigma, USA) and RNase (75 μg/ml, Sigma, USA) for 6 h in 37 ℃ water. Samples were rinsed with PBS thoroughly after each of these steps. Sterilization process was performed according to a two-step protocol suggested by Fidalgo et al. [24]: briefly, the samples were first treated with a mixed solution of vancomycin hydrochloride (50 mg/l), gentamicin (8 mg/l), cefoxitin (240 mg/l) and amphotericin B (25 mg/l) in PBS at 37 ℃ for 24 h under agitation (100 rpm), then treated with 0.1% (vol/vol) peracetic acid (used within 1 h of preparation) for 3 h with agitation (100 rpm) after adjusted to pH 7.3 with sodium hydroxide. Next, three washes (12 h for each) with PBS containing penicillin and streptomycin were performed with agitation (100 rpm).

2.2 Histological analysis

FP and AP were fixed in 4% paraformaldehyde solution for 24 h. After dehydration with graded ethanol and vitrification with dimethylbenzene, they were embedded in paraffin and were sectioned into 5 μm slices. The sections were dried, deparaffinized, rehydrated, and washed in distilled water. Hematoxylin and eosin (HE) staining was used to identify whether there were residual cell components in AP or not.

2.3 DNA detection

DNA contents in FP and AP were quantified using a Genomic DNA Extraction Kit (Takara, China) according to the manufacturer's instruction. Both FP (n=8) and AP (n=8) were cut into chips as small as possible, homogenated by a tissue tearor, and digested with Lysis Buffer, Proteinase K and RNase overnight in 56 ℃ water. The digested fluids were transferred into centrifugal columns, and DNA components that were absorbed on the silicon substrate membranes were finally dissolved in the TE buffer. The extracted DNA concentration was recorded using a P330 Ultramicrospectrophotometer (IMPLEN, Germany). The size of the extracted DNA fragments was detected by 1% agarose gel electrophoresis.

2.4 α-Gal epitopes quantification

Residual amounts of α-Gal epitopes in AP were quantified by enzyme-linked immunosorbent assay (ELISA) using a sheep α-Gal ELISA kit (MEIMIAN, China) in comparison with the amount in FP. FP samples (n=16) of the same weight (100 mg) were collected and half (n=8) were fabricated to AP. Tissue proteins in FP and AP were extracted by a One Step Animal Tissue Active Protein Extraction Kit (Sangon Biotech, China) according to the manufacturer's instructions. In brief, FP and AP were cut into chips as small as possible and homogenated with the help of ultrasound in the provided extraction, and then the supernatants were collected after centrifuged (13201 ×g, 10 min) at 4 ℃. α-Gal ELISA assay was then strictly conducted according to the manufacturer's instructions using aforementioned supernatants.

2.5 Residual SDS detection

Residual SDS was tested and calculated to make sure that no toxic substance was left in

AP. Standard SDS solutions with gradient concentrations were prepared and tested to draw a standard curve. AP (n=6) was incubated in PBS for 72 h at 37 ℃ and the supernatant was collected to prepare the extract liquor, which was tested using a Multiskan FC Spectrophotometer (Thermo, USA) at 499 nm.

2.6 Cell adhesion assay

AP were cut into a certain size which fits to the bottom area of one well in the 24-well plate and put into the 24-well plates with bone surface side up. Then, the 24-well plates were repackaged and irradiated by Cobalt 60 with an exposure dose of 15 kGy for the following use. Mouse MC3T3-E1 (Purchased from Cell center of basic medicine, Institute of Basic Medical Sciences of the Chinese Academy of Medical Sciences) were seeded onto the sterile AP (n=6) at a density of 2×10^4 cells/cm^2. After 6, 24, 48 h, cell culture supernatant was discarded and the cells were fixed for 24 h in 2.5% glutaraldehyde (Sigma, USA) solution. After rinsed three times with PBS (5 min each), the samples were dehydrated with graded ethanol (30%, 50%, 60%,70%, 80%, 90%,100% ethanol for 15 min each), and dried in hexamethyldisilazane (Sigma, USA). A thin layer of platinum alloy film was coated onto the surface of the samples for electrical conduction. The tissue samples were then viewed under a VEGA3 tungsten scanning electron microscope (TESCAN, Czech).

2.7 Cell proliferation assay

24-well plate equipped with AP was prepared as described in section 2.6. Mouse MC3T3-E1 cells were seeded onto the sterile AP at a density of 2×10^4 cells/cm^2 (n=9). Cells cultured in standard α-MEM culture medium (with 10% FBS) served as control. The cell proliferation assay of AP was determined by Cell Counting Kit-8 (CCK-8) at day 1, 3, 5 and 7. The absorbance was measured at 450 nm.

2.8 Alkaline phosphatase (ALP) activity

24-well plate equipped with AP was prepared as described in section 2.6. Mouse MC3T3-E1 cells were seeded onto the sterile AP at a density of 2×10^4 cells/cm^2 (n=9). Cells cultured without AP served as the control group. ALP activity in cell culture supernatant was determined via an ALP testing kit (NJJCbio, China) by reading optical density (OD) at 520 nm, and the results were expressed as King unit/100 ml. The time points subjected to analyses were day 3, 5, 7, 10, 14.

2.9 Quantitative real-time PCR

Total RNA was extracted from the recellularized AP (n=9) and the control group (n=9) using trizol according to the instructions of the manufacturer. Total RNA was reversely transcribed into cDNA using PrimeScript^{TM}RT reagent Kit with gDNA Eraser (RR047, Takara, Japan). Real-time PCR was performed in the LightCycler™ Real-Time PCR Detection System (Roche, Switzerland) using TB Green^{TM} Premix Ex TaqTM II (Tli RNaseH Plus) (RR820A, Takara, Japan). CT values were automatically obtained. Relative expression of mRNA amount was calculated using ΔΔCT method [25]. The time points subjected to analyses were day 7, 14, 21. The primers used for real-time PCR are listed in Table 1.

Table 1. Primers for real-time PCR analysis

Genes	**Sense primers (5'-3')**	**Antisense primers (5'-3')**	**Product Length (bp)**
Colla1	GACATGTTCAGCTTTGTGGACCTC	GGGACCCTTAGGCCATTGTGTA	119
Runx2	AGGGAATAGAGGGGATGCATTAG	AAGGGAGGACAGAGGGAAACA	104
Bglap2(OCN)	CGCCTACAAACGCATCTACG	CAGAGAGAGAGGACAGGGAGGA	118

β-actin	GTATCCTCGGATGTTGCTGCCTTG	CGCTGAGCATTGGTCCTCTTGG	101

2.10 Subcutaneous implantation tests

Animal experiment was performed according to protocols approved by the Institutional Animal Care and Use Committee at the China Medical University (No.2018035) and Local Ethical Committee for Laboratory Animals. Different membrane samples, including FP (positive control), AP and Bio-Gide (GEISTLICH, Switzerland) (one of clinical application products as negative control), were randomly implanted subcutaneously into the backs of a total of 60 six-month-old male SD rats (each rat with one sample of 1×1 cm^2). The rats were under general anesthesia using 3% sodium pentobarbital (30 mg/kg, IV). The back incision was located at the right side about 1.5-2 cm away from the central line, then the submucosa was separated from the right to the left, and the materials were implanted sub-mucously in the middle of the back. The distance between incision and right side of the material samples was set more than 1 cm long. After operation, the rats were housed individually in cages at a room temperature of 25 ℃. Four rats of each group were sacrificed by CO_2 at 3, 7, 14, 28 and 56 days after surgery. Blood was sampled from rat eyes to collect serum for ELISA using Quantikine IL-2 Elisa Kit (R&D, USA), Quantikine IL-4 Elisa Kit (R&D, USA) and IFN-γ Elisa Kit (NOVUS, USA). Grafts with adjacent tissues were cut off and fixed in 4% paraformaldehyde. Paraffin sections were made and dyed with HE staining which was used to mainly evaluate the host response to FP, AP and Bio-Gide. Immunohistochemical staining was performed to observe the change of density and distribution of macrophages around and within the three membranes. Briefly, sections were incubated with primary antibody against CD 11b (rabbit anti-CD 11b antibody, Abcam, Cambridge, MA) at 4 ℃

overnight after antigen retrieval, endogenous peroxidases inactivation and serum blocking. Then, the secondary antibody (goat anti-rabbit IgG1, Abcam, Cambridge, MA) was applied for 30 min after three times wash in PBS. After diaminobenzidine (DAB) chromogenic reaction and hematoxylin counterstaining, the slides were dehydrated, mounted, and imaged with OLYMPUS BX53 SYSTEM MICROSCOPE (OLYMPUS, Japan). Quantification of immunohistochemical staining was performed by using Image-Pro plus software. The number of CD 11b-positive cells were counted at 400 × and averaged over 5 areas per sample [26].

2.11 Statistical analysis

All quantitative data were expressed as means ± standard errors of the mean (SD). All collected data were analyzed using unpaired t-tests or one-way analyses of variance (ANOVA) with Tukey's post hoc test using SPSS 17.0 (Chicago, IL, USA) software. A confidence level of 95% ($p < 0.05$) was considered statistically significant.

3. Results

3.1 Confirmation of decellularization effectiveness and residual SDS amount

Fig. 2A-B shows the before and after decellularization macroscopic images of the same sheep periosteum. It turned from semitransparent to white and looked thicker and smaller after decellularization processes. HE staining image of Fig. 2C shows a two-layer structure of the fresh sheep periosteum. The inner thin layer, next to the bone tissue, was called cambium layer with a larger amount of cells distributing in the less tight structure; the outer thicker layer was called fibrous layer with less cells but well-organized collagen fibers aligned in the direction of bone growth. It was proved that no cell nucleus debris was observed after decellularization (Fig. 2D), while the arrangement of collagen fibers in AP remained as orderly as those in FP. The DNA quantitative assay suggested that the DNA amount in FP was 579.12 ± 35.87 ng/mg, while the amount of residual DNA after decellularization was 34.14 ± 6.86 ng/mg (Fig. 2E). No visible bands of DNA were observed after agarose gel electrophoresis in AP as compared to the whole genome bands in FP (Fig. 2F). α-Gal ELISA assay showed that the α-Gal content in AP (7.08 ± 1.64 ng/mg) was significantly lower than that in FP (35.80 ± 5.07 ng/mg) ($p < 0.05$) (Fig. 2G), which indicated that most of α-Gal epitopes were effectively removed during the decellularization process. Additionally, after thorough rinsing processes, residual SDS amount of AP was 0.0025%.

3.2 Effect of AP on cell adhesion

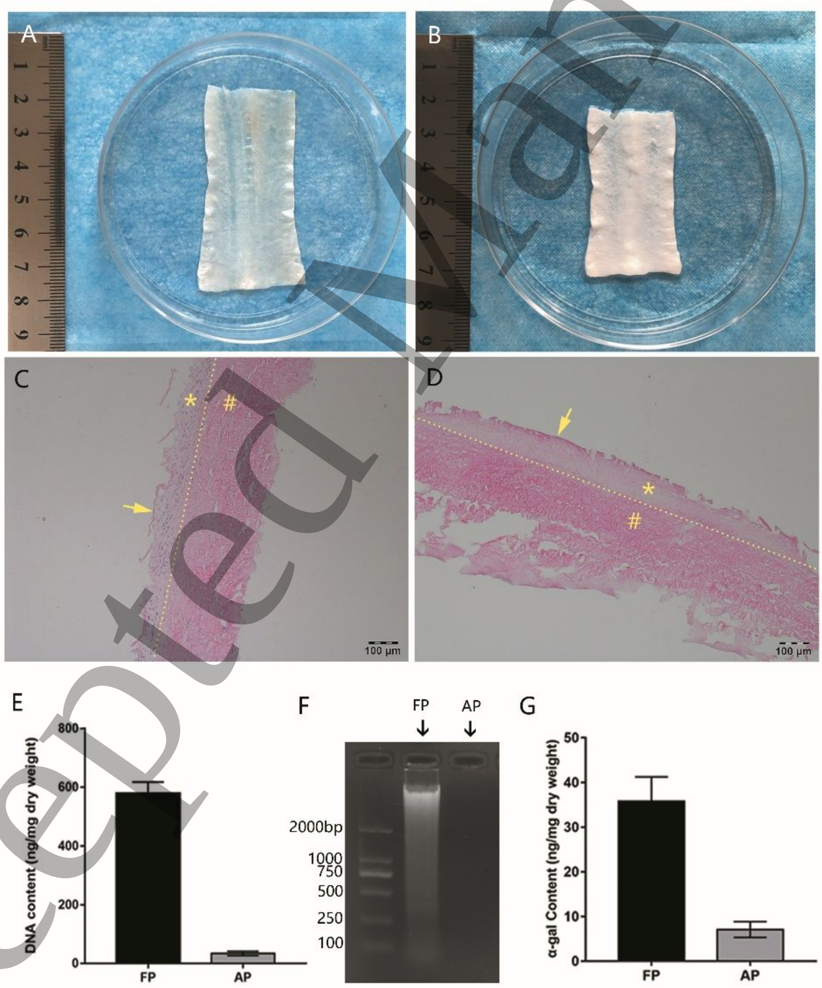

Fig. 2 Evaluation of the effectiveness of cell removal. Macroscopic images of FP (A) and AP (B), and confirmation of the removal of cells by HE staining (C: FP, D: AP, red arrow: the bone surface of the periosteum, #: fibrous layer, *: cambium layer), DNA quantitative detection (E), agarose gel electrophoresis (F) and α-gal quantitative detection (G).

The SEM images clearly showed that at 6 h, mouse MC3T3-E1 cells had already adhered onto the surface of AP with a lot of thin filamentous protein formation on the outer edge of the cells (Fig. 3A1-A3). At 24 h, mouse MC3T3-E1 cells gradually extended pseudopodia and turned from sphere into fusiform or polygon (Fig. 3B1-B3). At 48 h, they ultimately spreaded all over the membrane, and formed a new cell layer immediately on the surface of the membrane (Fig. 3C1-C3). These observations indicated that AP had a good biocompatibility by promoting cell adhesion.

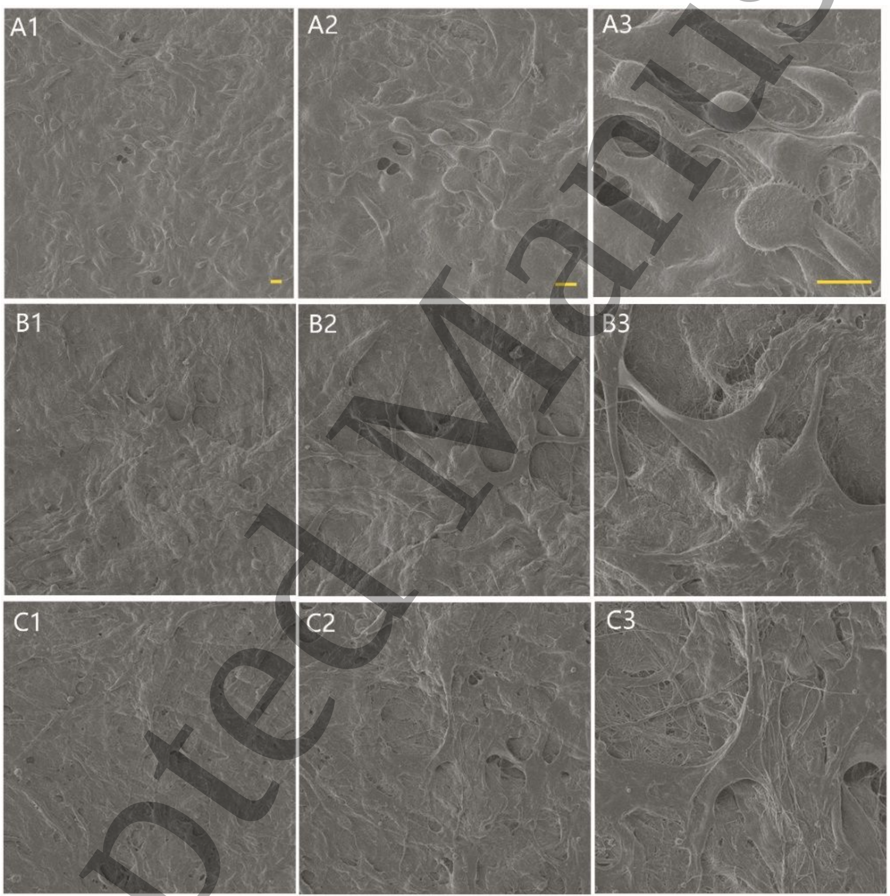

Fig. 3 SEM images of MC3T3-E1 cells adhesion on the surface of AP at 6 h (A1-A3), 24 h (B1-B3), 48 h (C1-C3) under different magnifications of × 1000 (A1, B1, C1), × 2000 (A2, B2, C2) and × 5000 (A3, B3, C3) (Scale bars = 10 μm).

3.3 Effect of AP on cell proliferation

The CCK-8 assay suggested that AP not only had zero toxic effect on mouse MC3T3-E1 cells but played a positive role in cell proliferation. Especially at day 5 and 7, the OD values of the experiment group (1.786±0.045 & 2.404±0.218) were significantly higher than the values of the control group (1.786±0.045 & 2.404±0.218) ($p < 0.05$) (Fig. 4A).

3.4 Effect of AP on cell osteogenic differentiation

The ALP activity in both groups showed an increasing trend along with the cell culture time and at each point-in-time, the ALP activity of cells seeded on AP was detected higher than each value in the control group, the superiority was quite obvious especially at day 3, 7 and 10 ($p < 0.05$) (Fig. 4B). Furthermore, the mRNA relative expression levels of Col I, Runx2 and OCN in the AP group were significantly higher than those in the control group to different degrees (Fig. 4C-E). At day 7, mRNA expression of Col I, Runx2, OCN in the AP group was 2.62-folder, 2.57-folder, 1.64-folder higher than the control group, respectively ($p < 0.05$). By day 14, the relative multiples respectively turned into 2.43-folder, 3.51-folder and 3.50-folder ($p < 0.05$). By day 21, there were still different degrees of improvement in the mRNA expression of Col I and OCN in

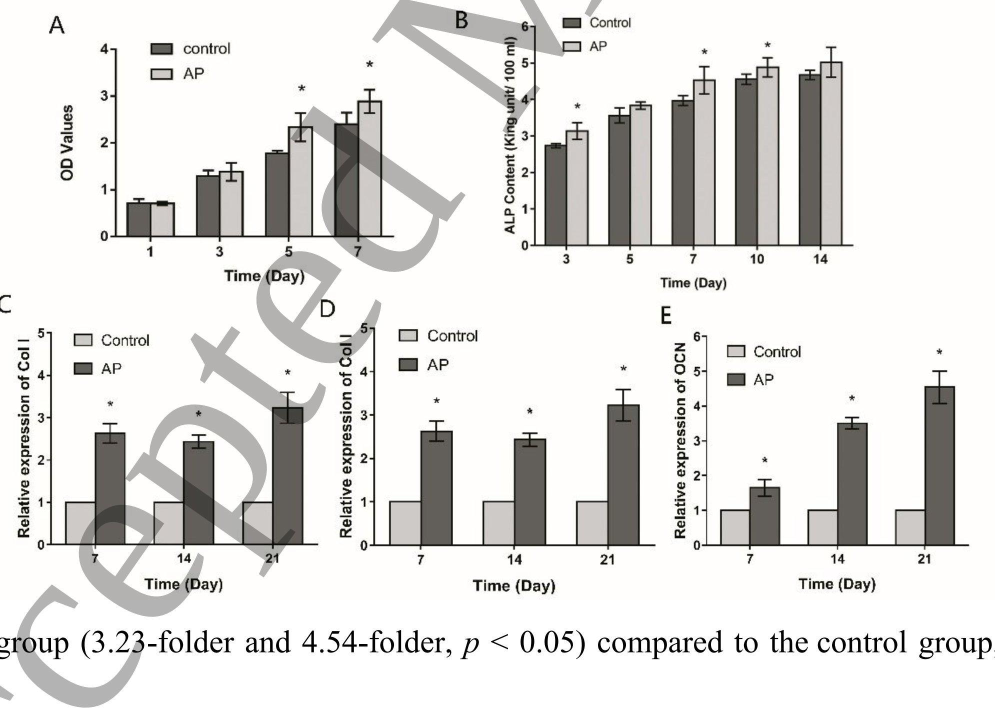

the AP group (3.23-folder and 4.54-folder, $p < 0.05$) compared to the control group, while the relative expression of Runx2 in the AP group decreased to 2.25-folder ($p < 0.05$), but it was still significantly higher than the control group.

Fig. 4 Levels of osteoblast proliferation and osteogenesis differentiation. OD values achieved from the CCK-8 assay reflected the mouse MC3T3-E1 cell proliferation on the surface of AP (A) (* $p < 0.05$). ALP activities were detected to determine the cell early differentiation capacity (B) (* $p < 0.05$). The mRNA relative expression levels of Col1 (C), Runx2 (D) and OCN (E) in the AP group were all significantly higher than those in the control group at day 7, 14 and 21 (* $p < 0.05$).

3.5 Subcutaneous implantation tests

All sixty rats survived until the point of scheduled time without complications. The ELISA assay of rat serum suggested that FP caused rise of IL-2 and IFN-γ in serum (Fig. 5A-B), which was significantly higher than the AP group and the Bio-Gide group at day 7, 14 and 28 ($p < 0.05$), while there was no significant difference between AP and Bio-Gide membrane. IL-4 content of the Bio-Gide group was a bit higher than the value of the FP group and the AP group at day 3, 7 and 14, but the difference was not of significance ($p > 0.05$) (Fig. 5C).

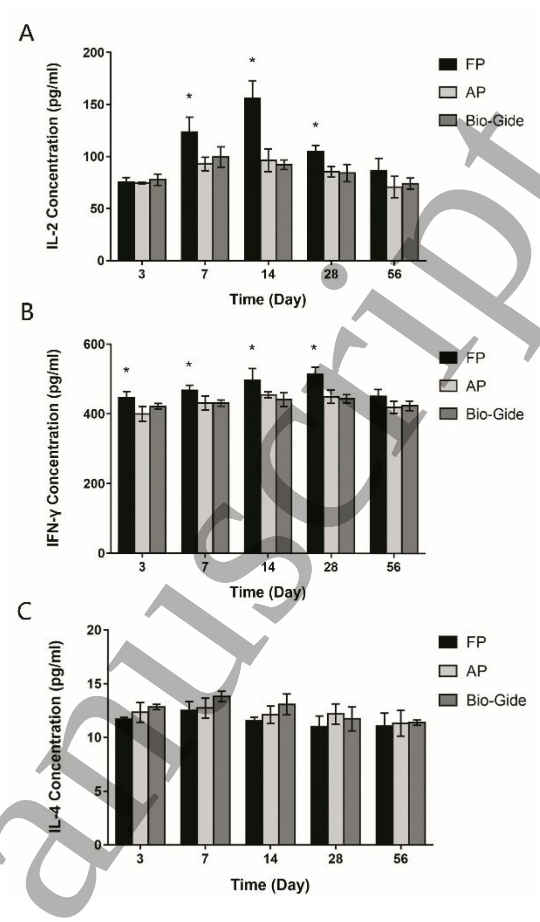

Fig. 5 IL-2, IFN-γ, IL-4 concentrations in serum of the SD rats subcutaneously implanted with FP, AP and Bio-Gide membranes (Compared with AP, * $p < 0.05$).

HE staining was conducted to demonstrate changes of inflammatory cell type, number and distribution after the membrane implantation. At day 3, a big quantity of inflammatory cells was infiltrating around the implanted FP with a large area of hemangiectasis and hyperemia, while the AP group and the Bio-Gide group presented only a few inflammatory cells around the contact areas and no obvious difference can be found between the two groups (Fig. 6A1-A3, 6a1-a3). At day 7, an increased infiltration of neutrophil cells and lymphocytes was observed aggregating towards the implanted FP region (Fig. 6B1 and 6b1), and in the AP group and the Bio-Gide group, the number of inflammatory cells also increased with lymphocytes as the primary cells (Fig. 6B2-B3 and 6b2-b3). By day 14, monocytes and mononuclear macrophages progressively increased in

Fig. 6 Histological observation of the subcutaneous implantation tests by HE staining. It shows the changing processes of inflammatory cell type and number as well as the integration of the grafts with the surrounding tissues at day 3, 7, 14, 28, 56 after implantation in the FP group, the AP group and the Bio-Gide group. Images with higher magnification (× 400) (Scale bar = 20 μm) represent the area within the black box in lower magnification images (× 100) (Scale bar = 100 μm).

the FP group, and the number of other types of inflammatory cells was still increasing as seen in Fig. 6C1 and 6c1. At the same time, the counts of lymphocytes in the AP group and the Bio-Gide group also increased and reached the peak, while edges of the membranes in two groups began to integrate with the surrounding tissues (Fig. 6C2-C3 and 6c2-c3). By day 28, the count and ratio of inflammatory cells in the FP group remained higher and most of them turned into lymphocytes (Fig. 6D1 and 6d1), while inflammatory cells around AP and the Bio-Gide membrane obviously decreased (Fig. 6D2-D3 and 6d2-d3). Till day 56, there were almost no inflammatory cells left in or around AP and the Bio-Gide membrane, and the membranes in the two groups were well integrated with the surrounding tissues (Fig. 6E2-E3 and 6e2-e3). However, there were still a lot more inflammatory cells flocking together in or around FP (Fig. 6E1 and 6e1).

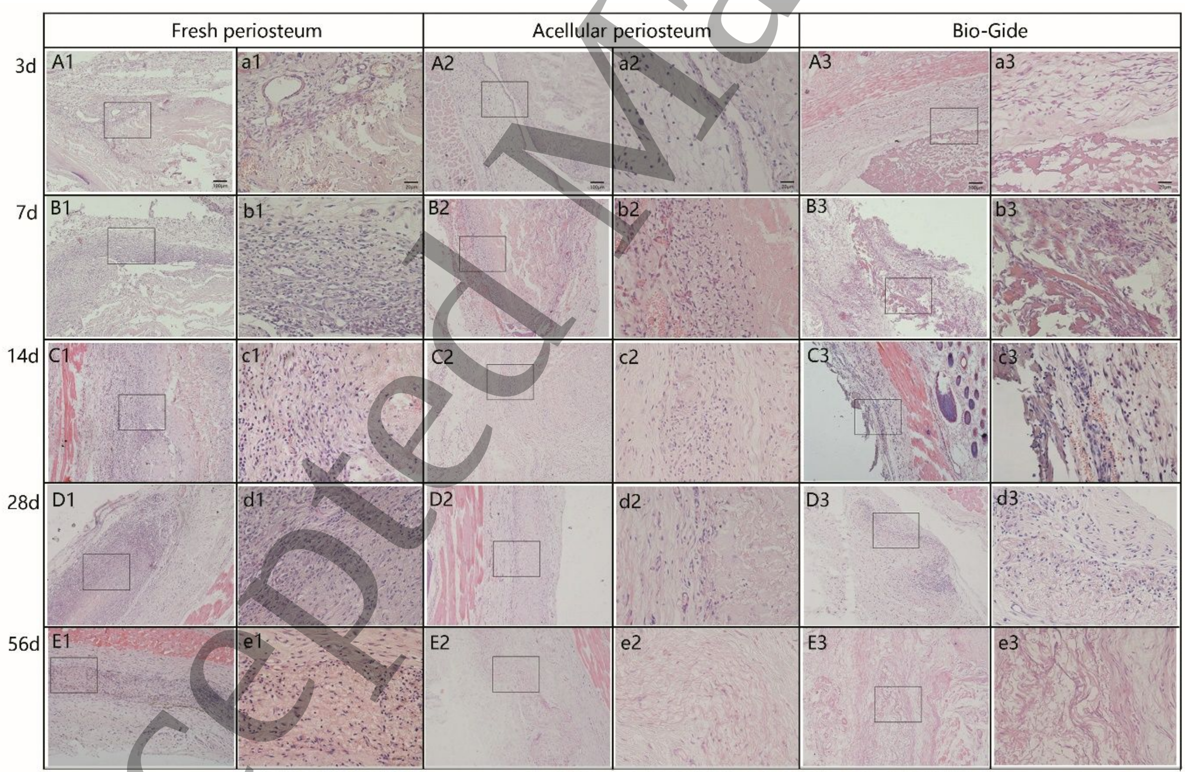

The immunohistochemical images mainly showed the role of CD 11b (+) macrophages in the process of foreign material implantation (Fig. 7A-E and 7a-e). Membranes were more easily distinguishable after the immunohistochemical staining that were characterized by light brown-

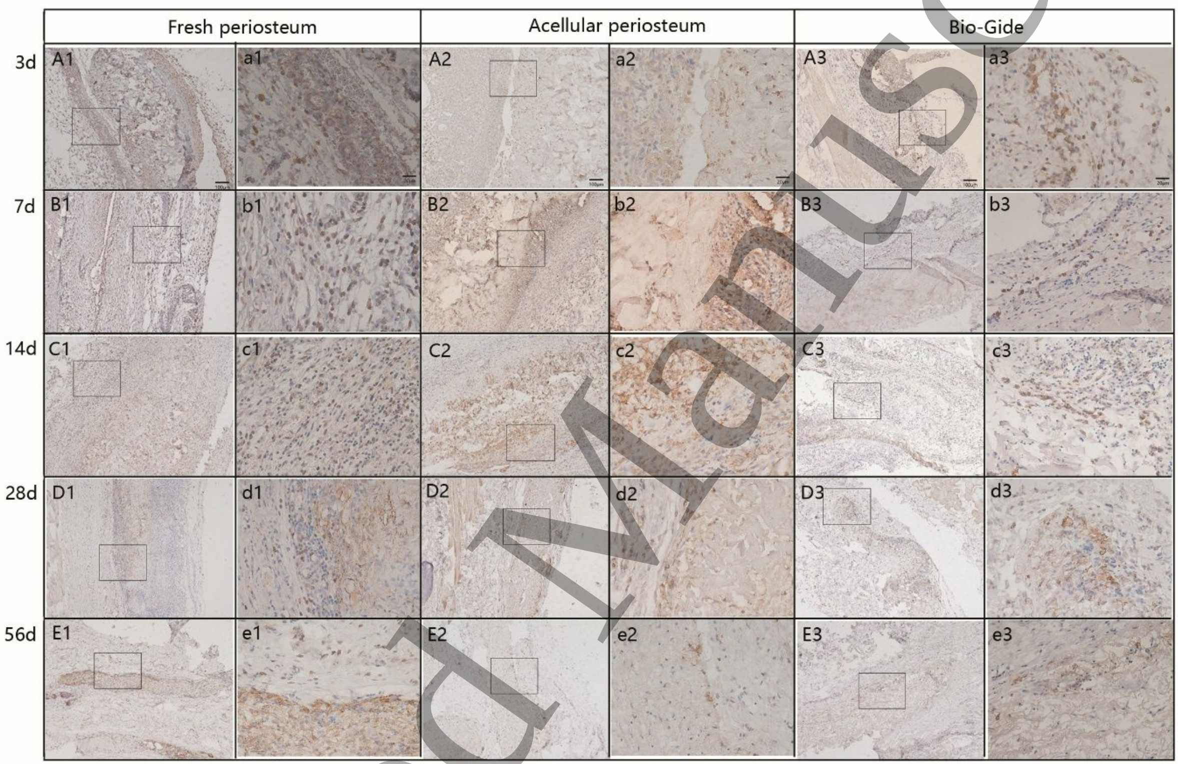

Fig. 7 Histological observation of the subcutaneous implantation tests by immunohistochemical staining. It shows the number and distribution of CD 11b (+) macrophages in the three groups during the healing process. Images with higher magnification (× 400) (Scale bar = 20 μm) represent the area within the black box in lower magnification images (× 100) (Scale bar = 100 μm).

stained zones, and cells of brown or pale brown stained in cytoplasm were regarded as CD 11b (+). In the FP group, CD 11b (+) cells began to sparsely appear in the adjacent tissues at day 3, and increased obviously at day 7 and 14, until day 28, CD 11b (+) cells presented less than before, and by day 56, the region where the membrane located remained rather dark with some still existing macrophages. While in the AP group and the Bio-Gide group, CD 11b (+) cells also followed the trend from increasing to decreasing, but CD 11b (+) cell counting was much lower

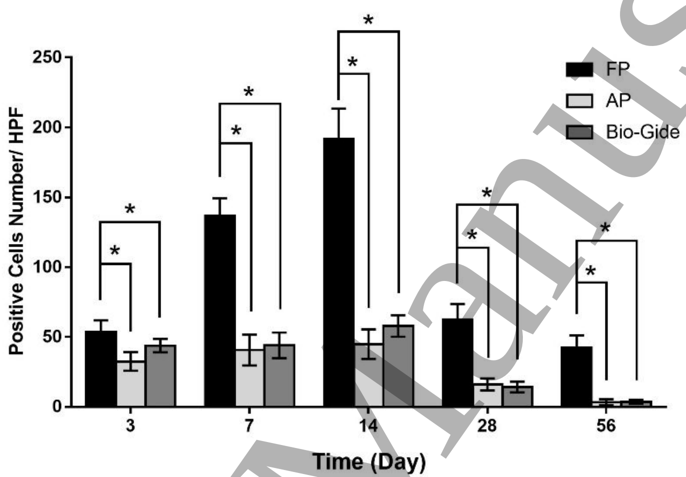

Fig.8 Quantification of immunohistochemical staining by positive cell counting at × 400 (* $p < 0.05$).

than that in the FP group, and after day 28, the color of the membrane-located areas was much lighter than before, and no obvious difference was found between the AP group and the Bio-Gide group. Quantitative analysis of the immunohistochemical images is shown in Fig. 8, significant differences could be found at each time point between FP and the other two groups.

4. Discussion

Native tissue-derived ECM, especially those site-specific homologous tissues [27], have been found more adaptable to the complexity of cell microenvironment than the synthetic materials [28]. As previous studies referring to physical and chemical characterization of ECM showed, it could also influence cell mitogenesis and chemotaxis, direct cell differentiation, and induce constructive host tissue remodeling responses [12, 23, 29, 30]. Therefore, ECM materials made from periosteum tissues were selected in the present study for conducting GBR research. Compared to the excessive thickness of the periostea of bovine or pig, the sheep periosteum is much thinner and its thickness is much closer to the current commercial GBR membranes. Additionally, it is also much easier to be dissected and harvested due to its simple anatomical structure.

There are variety of strategies to decellularize a particular tissue, including physical agents (freezing and thawing, agitation, ultrasound, pressure gradient, supercritical fluid), chemical agents (acids, bases, organic solvents, hypertonic solutions, ionic detergents, nonionic detergents) and enzymatic agents (trypsin, DNase and RNase, dispase, phospholipase A2). In most cases, these strategies are often applied in combination to enhance the effectiveness of decellularization process [31]. Taking into consideration that most of ionic detergents may be cytotoxic, besides the identical application of multigelation and DNase and RNase, we first tried hypertonic saline solution [32], octyl-glucopyranoside [33], which is a new kind of green detergent, and Triton X-100 alone. However, the results of our preliminary experiments showed that hypertonic saline solution, octyl-glucopyranoside surfactant and Triton X-100 alone all could not sufficiently disrupt or remove cells. Thus, taking the traditional chemical ionic detergent, a mild concentration of SDS was selected to use in combination with Triton X-100 in this study. As a result, we finally worked on removing the chemical agents by repeated washing with PBS, and the ultimate residual concentration of SDS in the 72-hour extract was 0.0025%, which was less than the absolute safe dose of the residual SDS amount (50mg/L, i.e., 0.005%) [34].

The widely-recognized standard for tissue decellularization was described by Crapo et al.

[12] as below: ① less than 50 ng dsDNA per mg ECM dry weight; ② less than 200 bp DNA fragment length; ③ lack of visible nuclear material in tissue sections stained with DAPI or HE. The results of our study entirely met the standard of the objective criteria: first, the residual DNA content in AP (32.52 ± 5.31 ng/mg dry weight) was less than 50 ng per mg ECM dry weight; Second, no visible DNA bands were observed after separation in 1% agarose gel, thus the longest DNA fragment length was surely less than 200 bp; Third, HE staining revealed the absence of visible nuclear components. These results proved that the decellularization protocol used in this study was efficient in removing cells from the periosteum tissue. Another important feature of decellularization is the reduction of antigenicity in the allogeneic and xenogeneic tissues. Alpha-gal, expressed in all mammalian tissues except humans and higher primates, is the major xenogeneic antigen epitope that induces complement-mediated cell lysis and hyper-acute rejection via human antibodies [35]. To the best of our knowledge, a quantitative standard has not been established for the safe range of residual α-Gal in the decellularized tissues. Wu et al. [36] detected residual amount of α-Gal in the acellular porcine annulus fibrosus scaffold by ELISA and found that α-Gal was removed by 67.24% mainly with SDS. The present study showed that the amount of α-Gal epitopes decreased 80.23% after decellularization, and the *in vitro* and *in vivo* tests confirmed that this residual amount was not enough to induce severe immunological rejection.

The biocompatibility of biological materials is an important consideration for their potential future applications. In the present study, it was systematically evaluated with respect to the capabilities of cell adhesion, proliferation, differentiation and osteogenesis. Cell adhesion was evaluated by visual inspection using fluorescence microscope and SEM. The whole process of cell adhesion was clearly observed from the SEM images with the morphological changes of mouse MC3T3-E1 cells, which gradually turned from sphere to fusiform and polygon, and linked with each other to form a new cell layer. To test the cytotoxicity and cell viability of AP, the CCK-8 test was performed and the results were interesting stating that the extracts not only had no toxic effect to the cells, but benefited the cell proliferation to some degree.

Similar results were obtained in the ALP activity test. ALP, which is an enzymatic protein expressed in the membrane of active osteoblasts, is essential for their ability to mineralize the extracellular matrix, especially in the early stage of osteogenesis differentiation [37]. In comparison with control group, the ALP activities of the experimental group were significantly higher at each time point from day 3 to 10, which indicated an increased ability of cell differentiation affected by AP. Subsequently, the mRNA expression of osteoblast-related genes was further detected from the mouse MC3T3-E1 cells cultured on AP. It was found that AP upregulated the mRNA expression levels of Col I, Runx2, OCN at 7, 14, 21 days. As a close-related osteogenesis gene expressed in the early stage of osteoblasts differentiation, Runx2 plays an important role in regulating the downstream genes for osteoblast differentiation and maturation, such as ALP and OCN [38]. In our study, Runx2 was expressed obvious high at day 14 in the AP group, and it declined at day 21, but its expression remained a little higher than the control group. The mRNA expressions of Col I and OCN in the AP group increased faster and higher than the control group from day 7, and by day 21, the expressions of Col I and OCN, respectively reached 3.23-folder and 4.54-folder higher values than the control group. One of the limited similar study was conducted by Li et al. [39], who demonstrated significantly higher mRNA expression of collagen type I, Runx2, ALP and OCN by using an 8-layer amnion-based scaffolds. According to all the results of *in vitro* studies obtained in our study, we strongly suggest that AP material could benefit pre-osteoblasts with good capacity of proliferation and osteogenic differentiation.

The existence of xenogeneic cell components left in the biomaterials has been suggested to potentially elicit an "inflammatory response" [40]. Hence, it is necessary to investigate the potential host immunoreaction to the AP material that we fabricated in this study prior to further *in vivo* studies. The effect of Th1 and Th2 lymphocytes in cell mediated immune response on xenografts has been reported as the fact that activation of Th1 pathway produces IL-2, IFN-γ and TNF-β which will result in macrophage activation, while Th2 lymphocyte response produces IL-4, IL-5, IL-6 and IL-10 and these cytokines will not activate macrophages. The Th1 pathway is associated with both allogeneic and xenogeneic transplant rejection, while the Th2 pathway is related to transplant acceptance [41]. The above research findings provide a potent support to our present study by stating that the SD rats implanted with FP presented a distinct increase in the values of the serum IL-2 (especially at day 7 and 14) and IFN-γ (especially before day 14), while the values in the AP group and the Bio-Gide group kept at a relatively low level, however, no significant difference was found in terms of IL-4 between the three groups. AP did not elicit immunological rejection via the Th1 pathway as FP did. Keane et al. [42] evaluated the effect of cell remnants within the biological scaffolds *in vivo* and discovered that the highest density of cell infiltration of the ineffective acellular group emerged at day 14, with swelling and seroma formation which was not observed in the effective acellular group and the concentration of macrophages reached to the peak at that time By day 28, the total numbers of infiltrating cells decreased but the proportion of macrophages remained similar to that at day 14. Our results are similar to those findings and we have further added three more time points of day 3, 7 and 56 for more comprehensive study. It was found in the FP group that infiltration of various inflammatory cells including the macrophages appeared earlier and was denser than those in the AP and Bio-Gide group, and those inflammatory cells even did not obviously decrease within the periosteum until 56 days post-surgery. Conversely, AP, which acted more like the Bio-Gide, presented a rather low-grade inflammation, which suggested that AP could not elicit an obvious immunogenic response. Besides, general observation of inserted AP and Bio-Gide was taken after 8 weeks when removed for histological analysis. AP was found to preserve relatively intact contour while Bio-Gide was barely noticeable at that time, which suggested that the degradation time of AP was much longer than the Bio-Gide. Taken together all above results, it is confirmed that AP possessed all properties of a favorable biological material and it could be tested in further *in vivo* osteogenesis experiments in future.

There were several limitations in the present study. Firstly, protein compositions in the AP material, including the category, and the amount of collagen, fibronectin, laminin and a variety of growth factors such as bone morphogenetic protein (BMP), vascular endothelial cell growth factor (VEGF), platelet derived growth factor (PDGF), etc. [41] were not systematically investigated in comparison with the native periosteum. Further studies for identifying the components of the AP-derived ECM are necessary to investigate the osteogenesis mechanism using liquid chromatography combined with mass spectroscopy method [43]. Secondly, *in vivo* effect detection of residual α-Gal was not included in the present study. As rats also wear α-Gal epitopes on all somatic cells and thus do not produce anti-α-Gal antibodies, further preclinical tests are considered by using models of α-Gal gene knockout rats or other experimental non-human primates. Thirdly, numerous studies have determined the macrophage polarization (M1/M2) while evaluating the inflammatory reactions of the subcutaneous implantation [42-44], which was not involved in the present study. More indexes are needed to be detected to uncover the possible mechanism in the transplant procedures of xenogeneic ECM. Although there are limitations, this study represents a systematic effort to determine the great application potentials of sheep AP in bone tissue engineering in terms of its biocompatibility.

5. Conclusion

The present study was the first to systematically investigate the biological performances of sheep AP *in vitro* and *in vivo*. The cellular compositions of AP were effectively removed. The AP material has different promoting effects on the adhesion, proliferation and osteogenesis differentiation of mouse MC3T3-E1 cells *in vitro*. No obvious immuno-inflammatory response occurred when AP was subcutaneously implanted into the backs of SD rats. In summary, with wider sources, less costs, more convenient fabrication process, acellular xenogeneic periostea would have great potential in the clinical application of GBR.

ACKNOWLEDGEMENTS

This work was supported by the National Key R&D Program of China [2017YFA0105802]; the National Natural Science Foundation of China [NO. 81771351]; and the Scientific Research Starting Foundation for Young Scientists of School of Stomatology, China Medical University [K101593-18-03].

REFERENCES

[1] Wessing B, Lettner S, Zechner W 2018 Guided Bone Regeneration with Collagen Membranes and Particulate Graft Materials: A Systematic Review and Meta-Analysis Int J Oral Maxillofac Implants 33 87-100

[2] Elgali I, Turri A, Xia W, Norlindh B, Johansson A, Dahlin C, Thomsen P, Omar O 2016 Guided bone regeneration using resorbable membrane and different bone substitutes: Early histological and molecular events Acta Biomater 29 409-23

[3] Dimitriou R, Mataliotakis G I, Calori G M, Giannoudis P V 2012 The role of barrier membranes for guided bone regeneration and restoration of large bone defects: current experimental and clinical evidence BMC Med 10 81

[4] Li N, Song J, Zhu G, Li X, Liu L, Shi X, Wang Y 2016 Periosteum tissue engineering-a review Biomater Sci 4 1554-61

[5] Reynders P, Becker J H, Broos P 1999 Osteogenic ability of free periosteal autografts in tibial fractures with severe soft tissue damage: an experimental study J Orthop Trauma 13 121-8

[6] Fan W, Crawford R, Xiao Y 2010 Enhancing in vivo vascularized bone formation by cobalt chloride-treated bone marrow stromal cells in a tissue engineered periosteum model Biomaterials 31 3580-9

[7] Shi X, Fujie T, Saito A, Takeoka S, Hou Y, Shu Y, Chen M, Wu H, Khademhosseini A 2014 Periosteum-mimetic structures made from freestanding microgrooved nanosheets Adv Mater 26 3290-6

[8] Rapp S J, Jones D C, Gerety P, Taylor J A 2012 Repairing critical-sized rat calvarial defects with progenitor cell-seeded acellular periosteum: a novel biomimetic scaffold Surgery 152 595-604, 5 e1; discussion -5

[9] Hoffman M D, Xie C, Zhang X, Benoit D S 2013 The effect of mesenchymal stem cells delivered via hydrogel-based tissue engineered periosteum on bone allograft healing Biomaterials 34 8887-98

[10] Hoffman M D, Benoit D S 2015 Emulating native periosteum cell population and subsequent paracrine factor production to promote tissue engineered periosteum-mediated allograft healing

Biomaterials 52 426-40

[11] Su W T, Chiou W L, Yu H H, Huang T Y 2016 Differentiation potential of SHEDs using biomimetic periosteum containing dexamethasone Mater Sci Eng C Mater Biol Appl 58 1036-45

[12] Crapo P M, Gilbert T W, Badylak S F 2011 An overview of tissue and whole organ decellularization processes Biomaterials 32 3233-43

[13] Somuncu O S 2019 Decellularization Concept in Regenerative Medicine Adv Exp Med Biol

[14] Bejleri D, Davis M E 2019 Decellularized Extracellular Matrix Materials for Cardiac Repair and Regeneration Adv Healthc Mater e1801217

[15] Thampi P, Nair D, R L, N V, Venugopal S, Ramachandra U 2013 Pathological effects of processed bovine pericardial scaffolds--a comparative in vivo evaluation Artif Organs 37 600-5

[16] Gates K V, Dalgliesh A J, Griffiths L G 2017 Antigenicity of Bovine Pericardium Determined by a Novel Immunoproteomic Approach Sci Rep 7 2446

[17] Vadori M, Cozzi E 2015 The immunological barriers to xenotransplantation Tissue Antigens 86 239-53

[18] Dalgliesh A J, Parvizi M, Lopera-Higuita M, Shklover J, Griffiths L G 2018 Graft-specific immune tolerance is determined by residual antigenicity of xenogeneic extracellular matrix scaffolds Acta Biomater 79 253-64

[19] Cheng C W, Solorio L D, Alsberg E 2014 Decellularized tissue and cell-derived extracellular matrices as scaffolds for orthopaedic tissue engineering Biotechnol Adv 32 462-84

[20] Ngo M D, Aberman H M, Hawes M L, Choi B, Gertzman A A 2011 Evaluation of human acellular dermis versus porcine acellular dermis in an in vivo model for incisional hernia repair Cell Tissue Bank 12 135-45

[21] Huang H, Xiao H, Liu H, Niu Y, Yan R, Hu M 2015 A comparative study of acellular nerve xenografts and allografts in repairing rat facial nerve defects Mol Med Rep 12 6330-6

[22] Huang X, Zhu Q, Jiang L, Zheng C, Zhu Z, Lu Q, Xu Y, Gu L, Liu X 2012 [Study on immune response after repair of nerve defect with acellular nerve xenograft laden with allogenic adipose-derived stem cells in rhesus monkey] Zhongguo Xiu Fu Chong Jian Wai Ke Za Zhi 26 993-1000

[23] He J, Li Z, Yu T, Wang W, Tao M, Ma Y, Wang S, Fan J, Tian X, Wang X, Lin Y, Ao Q 2019 Preparation and evaluation of acellular sheep periostea for guided bone regeneration J Biomed Mater Res A

[24] Fidalgo C, Iop L, Sciro M, Harder M, Mavrilas D, Korossis S, Bagno A, Palu G, Aguiari P, Gerosa G 2018 A sterilization method for decellularized xenogeneic cardiovascular scaffolds Acta Biomater 67 282-94

[25] Livak K J, Schmittgen T D 2001 Analysis of relative gene expression data using real-time quantitative PCR and the 2(-Delta Delta C(T)) Method Methods 25 402-8

[26] Wang X, Zhou Y, Peng Y, Huang T, Xia F, Yang T, Duan Q, Zhang W 2019 Bromodomain-containing protein 4 contributes to renal fibrosis through the induction of epithelial-mesenchymal transition Exp Cell Res 383 111507

[27] Zhang Y, He Y, Bharadwaj S, Hammam N, Carnagey K, Myers R, Atala A, Van Dyke M 2009 Tissue-specific extracellular matrix coatings for the promotion of cell proliferation and maintenance of cell phenotype Biomaterials 30 4021-8

[28] Gilpin A, Yang Y 2017 Decellularization Strategies for Regenerative Medicine: From Processing Techniques to Applications Biomed Res Int 2017 9831534

[29] Subbiah R, Du P, Van S Y, Suhaeri M, Hwang M P, Lee K, Park K 2014 Fibronectin-tethered

graphene oxide as an artificial matrix for osteogenesis Biomed Mater 9 065003

[30] Subbiah R, Hwang M P, Du P, Suhaeri M, Hwang J H, Hong J H, Park K 2016 Tunable Crosslinked Cell-Derived Extracellular Matrix Guides Cell Fate Macromol Biosci 16 1723-34

[31] Gupta S K, Mishra N C, Dhasmana A 2017 Decellularization Methods for Scaffold Fabrication Methods Mol Biol

[32] Shafiq M A, Gemeinhart R A, Yue B Y, Djalilian A R 2012 Decellularized human cornea for reconstructing the corneal epithelium and anterior stroma Tissue Eng Part C Methods 18 340-8

[33] Dong J, Li Y, Mo X 2013 The study of a new detergent (octyl-glucopyranoside) for decellularizing porcine pericardium as tissue engineering scaffold J Surg Res 183 56-67

[34] Cebotari S, Tudorache I, Jaekel T, Hilfiker A, Dorfman S, Ternes W, Haverich A, Lichtenberg A 2010 Detergent decellularization of heart valves for tissue engineering: toxicological effects of residual detergents on human endothelial cells Artif Organs 34 206-10

[35] Abdel-Motal U M, Wigglesworth K, Galili U 2009 Mechanism for increased immunogenicity of vaccines that form in vivo immune complexes with the natural anti-Gal antibody Vaccine 27 3072-82

[36] Wu L C, Kuo Y J, Sun F W, Chen C H, Chiang C J, Weng P W, Tsuang Y H, Huang Y Y 2017 Optimized decellularization protocol including alpha-Gal epitope reduction for fabrication of an acellular porcine annulus fibrosus scaffold Cell Tissue Bank 18 383-96

[37] Deng B, Bruzzaniti A, Cheng G J 2018 Enhancement of osteoblast activity on nanostructured NiTi/hydroxyapatite coatings on additive manufactured NiTi metal implants by nanosecond pulsed laser sintering Int J Nanomedicine 13 8217-30

[38] Komori T 2005 Regulation of skeletal development by the Runx family of transcription factors J Cell Biochem 95 445-53

[39] Li W, Ma G, Brazile B, Li N, Dai W, Butler J R, Claude A A, Wertheim J A, Liao J, Wang B 2015 Investigating the Potential of Amnion-Based Scaffolds as a Barrier Membrane for Guided Bone Regeneration Langmuir 31 8642-53

[40] Zheng M H, Chen J, Kirilak Y, Willers C, Xu J, Wood D 2005 Porcine small intestine submucosa (SIS) is not an acellular collagenous matrix and contains porcine DNA: possible implications in human implantation J Biomed Mater Res B Appl Biomater 73 61-7

[41] Badylak S F 2004 Xenogeneic extracellular matrix as a scaffold for tissue reconstruction Transpl Immunol 12 367-77

[42] Keane T J, Londono R, Turner N J, Badylak S F 2012 Consequences of ineffective decellularization of biologic scaffolds on the host response Biomaterials 33 1771-81

[43] Schneider K H, Enayati M, Grasl C, Walter I, Budinsky L, Zebic G, Kaun C, Wagner A, Kratochwill K, Redl H, Teuschl A H, Podesser B K, Bergmeister H 2018 Acellular vascular matrix grafts from human placenta chorion: Impact of ECM preservation on graft characteristics, protein composition and in vivo performance Biomaterials 177 14-26

[44] Ballotta V, Driessen-Mol A, Bouten C V, Baaijens F P 2014 Strain-dependent modulation of macrophage polarization within scaffolds Biomaterials 35 4919-28